Global Increase of Near- and Below-Barrier Fusion for Heavier Systems

U. Jahnke, H. H. Rossner, D. Hilscher, and E. Holub
Hahn-Meitner-Institut für Kernforschung, D-1000 Berlin 39, Germany
(Received 2 September 1981)

Twenty excitation functions for ^{12}C-, ^{16}O-, ^{40}Ar-, and ^{86}Kr-induced fusion were deduced from measured neutron production cross sections. A global increase of the near-barrier fusion is observed as reactant masses increase, which by far cannot be accounted for by one-dimensional barrier penetration models. Static properties such as deformation introduce only small modifications to this tendency, whereas the mean curvature radius provides a good scaling to this phenomenon, thus indicating shape distortions or neck formation.

PACS numbers: 25.70.Bc, 25.70.Fg

In the low-energy domain above the barrier the classical one-dimensional picture of two hard spheres fusing after a touching collision provides an excellent description for the fusion cross section, simply because the majority of the trajectories lead to fusion irrespective of shape distortions, induced vibrations and rotations, or nucleon transfer which might have preceded. The fusion cross section—cumulative in angular momentum—is not sensitive to these degrees of freedom though they indeed may be strongly excited as might be inferred from the analogous fission process. It is only in the vicinity of the barrier that the energy balance might be affected so drastically as to have an observable effect on the fusion probability. Similarly, specific nuclear-structure properties such as static deformation or deformability are expected to be most effective near the barrier.

Because of the difficulties inherent in low cross-section experiments, investigations have so far rather been restricted to identifying the effect of static deformation[1-3] or recently the influence of valence neutrons[4] on a limited number of systems. Though the experiments, including those with light ions,[5] did not succeed in unambiguously quantifying the influence of nuclear structure, they showed, however, that the large near-barrier cross sections observed for heavier systems cannot be accounted for by static properties only. The present state of experimental and theoretical efforts in this field is summarized in a recent review by Vaz, Alexander, and Satchler.[6]

The intention of this paper is to show on a comparative basis that the near-barrier fusion probability globally increases for heavier systems, i.e., for systems with larger curvature radii, whereas the relative influence of nuclear structure seems to diminish. This is the predominant result of twenty fusion excitation functions obtained with ^{12}C, ^{16}O, ^{40}Ar, and ^{86}Kr beams on target nuclei in the mass range $A = 12-154$ (Table I). A new experimental method has been applied which is very well suited for a general survey because of its relative ease and low beam time consumption: Instead of detecting the heavy residues, which for heavier systems are increasingly focused into a narrow and, for conventional techniques, hardly accessible cone around the beam direction, we detect the neutron evaporation yield from the fused system and convert this yield to the fusion cross section by dividing it by the calculated average number of neutrons emitted per fusion event.

The experiments have been performed with the internal beam of the VICKSI cyclotron at the Hahn-Meitner-Institut. In this cyclotron the beam from a 6-MV Van de Graaff injector is accelerated in some 80 to 150 very well defined and separated turns with an energy gain of 2 to 4 MeV per turn. The excitation functions could thus be measured internally by setting the target assembly at the end of a radial probe shaft from one turn to the next. The neutron yield was detected by two flat-

TABLE I. List of investigated systems together with the extracted barrier heights V_B (in MeV).

System	V_B	System	V_B
$^{40}Ar + ^{12}C$	16.2 ± 0.2	$^{40}Ar + ^{62}Ni$	65.1 ± 0.6
$^{40}Ar + ^{16}O$	21.0 ± 0.3	$^{40}Ar + ^{64}Ni$	63.9 ± 0.5
$^{12}C + ^{110}Pd$	35.1 ± 0.3	$^{40}Ar + ^{104}Pd$	98.1 ± 0.8
$^{12}C + ^{124}Sn$	37.4 ± 0.3	$^{40}Ar + ^{110}Pd$	97.4 ± 0.9
$^{12}C + ^{130}Te$	38.6 ± 0.3	$^{40}Ar + ^{118}Sn$	105.6 ± 0.7
$^{16}O + ^{110}Pd$	46.2 ± 0.3	$^{40}Ar + ^{124}Sn$	104.3 ± 0.8
$^{16}O + ^{144}Sm$	59.9 ± 0.5	$^{40}Ar + ^{130}Te$	108.5 ± 0.8
$^{16}O + ^{154}Sm$	58.5 ± 0.4	$^{86}Kr + ^{58}Ni$	120.8 ± 1.1
$^{40}Ar + ^{58}Ni$	65.3 ± 0.5	$^{86}Kr + ^{62}Ni$	119.3 ± 0.8
$^{40}Ar + ^{60}Ni$	65.5 ± 0.6	$^{86}Kr + ^{64}Ni$	118.3 ± 0.7

energy-response BF_3 counters fixed inside the cyclotron vacuum chamber at angles of 100 to 120 degrees to the beam direction depending on the radial position of the target. The efficiency and the solid angle of the detectors were calibrated by replacing the target by ^{252}Cf and Pu-Be neutron sources of known strength. The energy of the ion beam in the different orbits was calculated from measured orbit positions, the known magnetic field distribution, and the revolution frequency. For Ne, Ar, and Kr beams the energy was also measured in several orbits with a proton recoil detector[7] thereby confirming the calculation within the experimental accuracy of 0.6%. Thin targets (20–120 $\mu g/cm^2$) were prepared by vacuum evaporation of isotopically enriched materials (> 95%) onto 0.5-mm-thick gold backings. Cross sections were referred to weighted target thicknesses and integrated beam currents.[8]

As typical examples we give in Fig. 1 our results for the systems $^{16}O+^{154}Sm$ and $^{40}Ar+^{110}Pd$ for which both the fusion cross sections and the neutron multiplicities have been measured elsewhere[2,9] with different techniques. The data evaluation consisted in a three-step procedure: (i) subtraction of background, (ii) normalization and angular integration to provide the total neutron-emission cross sections displayed in the upper part of the figure, and (iii) division by the calculated average neutron multiplicity $\langle n(E)\rangle$ in the middle part to yield the fusion excitation functions exhibited at the bottom.

Special attention was paid to the background originating from 1- to 2-$\mu g/cm^2$ carbon contamination. During the experiment the contamination was identified by its threshold for neutron emission and its quantity deduced by comparing the neutron yield to that of carbon targets of known thickness.

Total neutron-production cross sections were obtained by calculating the angular distributions according to the simple formula for the weak-coupling case given by Ericson and Strutinski.[10] The angular integrations as well as corrections applied for the backscattering of the neutrons from the magnet iron were verified by measuring angular distributions with extracted ^{40}Ar and ^{86}Kr beams on a sample of light and heavy targets.

Average multiplicities $\langle n(E)\rangle$ were calculated as a function of incident energy from the statistical evaporation model implicitly with the assumption that neutrons originate from compound-nucleus evaporation only. This assumption seems

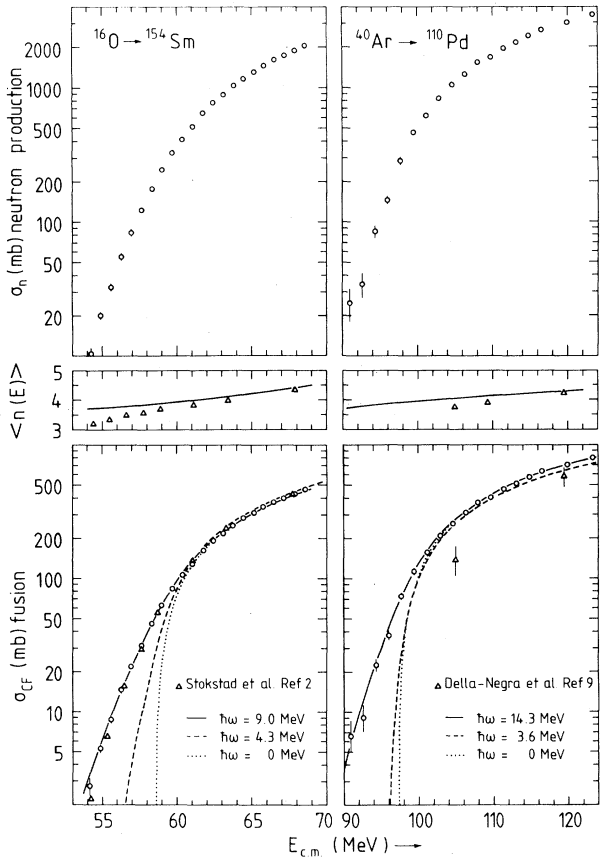

FIG. 1. Experimental neutron-production cross sections, calculated neutron multiplicities $\langle n(E)\rangle$ (full lines), and deduced fusion excitation functions for the systems $^{16}O+^{154}Sm$ and $^{40}Ar+^{110}Pd$. Circles represent the results of the present study, triangles those of Refs. 2 and 9. In the bottom part the full lines are the fits according to Eq. (1); the dotted lines show the reduction of the cross section when penetration is not considered ($\hbar\omega = 0$). The dashed lines denote full barrier-penetration calculations (Ref. 17) with the proximity potential, shifted in energy, however, so as to give the same barrier heights as the experiment.

to be very well justified in our energy domain since the competing Coulomb and inelastic excitation or transfer processes are not likely to release neutrons. The calculations were performed with the code MBII,[11] using the same set of standard parameters for all systems. From a comprehensive comparison with published xn cross section data (see also Gavron[12]) we conclude that, though there may be a considerable discrepancy for specific xn channels, the calculated average $\langle n\rangle$ is reliable to within 15%. Since the calculation would probably be less certain for very neutron-deficient systems or when fission contributes to the compound-nucleus decay, the ex-

periments have been restricted to a mass and energy region (composite mass $\lesssim 170$, $l_{max} \lesssim 65$) where primary neutron evaporation is dominant.

The fusion excitation functions derived from $\sigma_{cf}(E) = \sigma_n(E)/\langle n(E)\rangle$ for $^{16}O + ^{154}Sm$ in Fig. 1 are in very satisfactory agreement with the results of Stokstad *et al.*[2] For $^{40}Ar + ^{110}Pd$ we observe a considerable discrepancy with the data of Della-Negra *et al.*[9] We estimate the uncertainty in the absolute cross section to be about 20%. The error bars in Fig. 1 account for counting statistics and background subtraction only.

In order to compare quantitatively the relative size of the subbarrier cross sections observed for the different systems, we parametrize the excitation functions with the Wong[13] formula. This formula extends the simple sharp-cutoff relation $\sigma_{cf} = \pi R_B^2(1 - V_B/E_{c.m.})$ by a close-to-exponential tail into the subbarrier region

$$\sigma_{cf} = \frac{R_B^2 \hbar\omega}{2E_{c.m.}} \ln\left(1 + \exp 2\pi \frac{E_{c.m.} - V_B}{\hbar\omega}\right). \quad (1)$$

For fixed barrier height V_B and position R_B the tail in (1) essentially grows with $\hbar\omega$, which we therefore name "tail strength" parameter. In the original concept it allows for quantum mechanical penetration of a static one-dimensional potential barrier as approximated for $l = 0$ by an inverted parabola with curvature $\hbar\omega$. Analytically this three-parameter form provides an adequate description for the data: In the upper energy region $E_{c.m.} \gtrsim V_B + \frac{1}{4}\hbar\omega$, the $1/E_{c.m.}$ dependence is rather well confirmed as is the close-to-exponential tailing in the threshold region. Only at very low cross sections $\sigma_{cf} < 10$ mb do the data for some systems seem to decrease faster than provided by (1). Examples of the fit are included in Fig. 1. In agreement with Ref. 6 we used the range of σ_{cf} from 100 to 500 mb for the determination of V_B, listed in Table I. The error bars quoted in Table I and in Fig. 2 for $\hbar\omega$, however, allow for the variation of V_B and $\hbar\omega$ when lower limits between 100 and 200 mb are used. As a result of the interdependence of the parameters V_B and $\hbar\omega$ in (1) the majority of the published experimental data cannot be included in the present consideration because their energy span either below or above the barrier is too limited.

The tail strengths $\hbar\omega$ for the different systems are plotted in Fig. 2 versus their mean curvature or "reduced" radii[14] $\bar{R} = C_1C_2/(C_1 + C_2)$. The hatched area indicates the widths $\hbar\omega$ of the $l = 0$ potential barriers in the parabolic approximation when calculating the nuclear potential from the

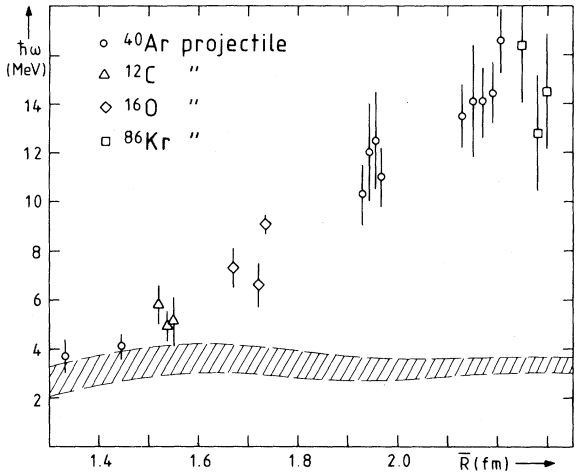

FIG. 2. Strength of the subbarrier tailing of the fusion cross section observed for the systems listed in Table I in the order of increasing mean curvature radii $\bar{R}$. The hatched band indicates $l = 0$ barrier widths for various nuclear potential models.

currently most often used proximity,[14] the Yukawa-plus-exponential,[15] or the Bass model[16] and approximating the Coulomb part by a point-plus-spherical charge distribution. For the two examples in Fig. 1 we also show the full barrier-penetration calculation[17] for σ_{cf}, i.e., a calculation which within the parabola approximation unlike (1) allows for the inward shift and broadening of the potential barrier for higher partial waves—referring to the proximity potential.

It is immediately obvious from the contrast between experiment and calculation in Figs. 1 and 2 and has already been pointed out by Refs. 1, 3, and 6 that the tail strength $\hbar\omega$ can originate from potential-barrier penetration only for the very light systems, e.g., $^{40}Ar + ^{12}C, ^{16}O$—the deformed ^{12}C showing no enhancement over the spherical ^{16}O target. From then on we observe a continuous and steady growth of the tail for heavier systems, the discrepancy with the barrier-penetration calculation becoming so large that by no means can it be attributed to the deficiencies of the parabola approximation to the real potential.[6] For the heaviest systems in Fig. 2 the tail strength, if still related to the width of a static barrier, would indicate such narrow barriers that they could not even be produced by a square well for the nuclear attraction.

There is also a considerable scattering about this overall tendency, though mostly within the present experimental accuracy. This scattering can be related to either static deformations or

the presence of loosely bound neutrons as might be inferred from the sequences $^{16}O+^{144,154}Sm$, $^{40}Ar+^{58,60,62,64}Ni$, and $^{86}Kr+^{58,62,64}Ni$, or to the nuclear stiffness which is believed to change appreciably within the series $^{12}C+Pd,Sn,Te$, and $^{40}Ar+Pd,Sn,Te$ when crossing the $Z=50$ shell closure. However, the intrinsic nuclear structure of the colliding nuclei does not drastically offset the general increase of the near-barrier cross section. Moreover, its relative significance seems to diminish the heavier the systems. The data for ^{35}Cl, $^{40}Ca+^{58,\ldots,64}Ni$ and $^{40}Ar+^{144,148,154}Sm$ (Refs. 1 and 3), if analyzed in a similar way, would not invalidate the present systematics.

In conclusion, we find that heavy-ion fusion in the near-barrier regime by far exceeds the prediction of the simple concept of a potential barrier which depends on the separation coordinate only. The excess shows a global increase for heavier systems. The reduced radius of the coalescing system, reflecting the size of the opposing surfaces, provides a good scaling[18] to this phenomenon thus indicating shape distortion or neck formation.

[1]B. Sikora *et al.*, Phys. Rev. C 20, 2219 (1979).
[2]R. G. Stokstad *et al.*, Phys. Rev. C 21, 2427 (1980).
[3]R. G. Stokstad *et al.*, Z. Phys. A 295, 269 (1980).
[4]M. Beckermann *et al.*, Phys. Rev. Lett. 45, 1472 (1980).
[5]H. Freiesleben and J. R. Huizenga, Nucl. Phys. A224, 503 (1974).
[6]L. C. Vaz, J. M. Alexander, and G. R. Satchler, Phys. Rep. 69, 373 (1981).
[7]D. K. Olsen *et al.*, Nucl. Instrum. Methods 114, 615 (1974).
[8]A complete description of the experiment and detailed results will be given in a forthcoming article.
[9]S. Della-Negra *et al.*, Z. Phys. A 282, 65 (1977); the discrepancy could be resolved by a reported shift of 4 MeV [R. L. Hahn *et al.*, Phys. Rev. Lett. 42, 218 (1979)] associated with the absorber method.
[10]T. Ericson and V. Strutinski, Nucl. Phys. 8, 284 (1958).
[11]M. Beckerman and M. Blann, Phys. Rev. C 17, 1615 (1978).
[12]A. Gavron, Phys. Rev. C 21, 230 (1980).
[13]C. Y. Wong, Phys. Rev. Lett. 31, 766 (1973).
[14]J. Blocki, J. Randrup, W. J. Swiatecki, and C. F. Tsang, Ann. Phys. (N.Y.) 105, 427 (1977).
[15]H. J. Krappe, J. R. Nix, and A. J. Sierk, Phys. Rev. C 20, 992 (1979).
[16]R. Bass, Phys. Rev. Lett. 39, 265 (1977).
[17]L. C. Vaz, computer code FRANPIE, to be published.
[18]Probably better than the mass or charge product or related parameters, as might be inferred from $^{16}O+Pd,Sm$ and $^{40}Ar+Ni$.

Detection of the Infrared Fundamental Band of HeH^+

P. Bernath and T. Amano
Herzberg Institute of Astrophysics, National Research Council of Canada, Ottawa K1A 0R6, Canada
(Received 5 November 1981)

Nine vibration-rotation transitions of the fundamental band of HeH^+ have been observed in absorption by using a tunable, infrared, difference-frequency laser source. The molecular constants for the $v=0$ and $v=1$ levels of the $X\,^1\Sigma^+$ state have been determined and they agree very will with those derived from the *ab initio* calculation of Bishop and Cheung.

PACS numbers: 33.20.Ea, 35.20.Pa, 36.90.+f

Recently Oka[1] observed the vibration-rotation spectrum of H_3^+ using a tunable infrared source made by mixing radiation from an argon-ion laser and a dye laser in a $LiNbO_3$ crystal.[2] It was suggested by Oka that other ions might be detected with similar methods. We would like to report the observation of nine lines, $P(4)(J=3\leftarrow4)$ to $R(4)(J=5\leftarrow4)$, of the fundamental band ($v=1\leftarrow0$) of HeH^+.

HeH^+ is the simplest closed-shell heteronuclear molecule and is isoelectronic with H_2. Because the two most abundant elements in the universe are hydrogen and helium, it is not surprising that HeH^+ has been subjected to intense theoretical and considerable experimental scrutiny.[3,4]

Hogness and Lunn[5] discovered HeH^+ in 1924

